

Forward and Reverse Genetics through Derivation of Haploid Mouse Embryonic Stem Cells

Ulrich Elling,¹ Jasmin Taubenschmid,¹ Gerald Wirnsberger,¹ Ronan O'Malley,² Simon-Pierre Demers,³ Quentin Vanhaelen,³ Andrey I. Shukalyuk,⁴ Gerald Schmauss,¹ Daniel Schramek,¹ Frank Schnuetgen,⁵ Harald von Melchner,⁵ Joseph R. Ecker,^{2,6} William L. Stanford,^{3,4,7} Johannes Zuber,⁸ Alexander Stark,⁸ and Josef M. Penninger^{1,*}

¹IMBA, Institute of Molecular Biotechnology of the Austrian Academy of Sciences, 1030 Vienna, Austria

²Genomic Analysis Laboratory, The Salk Institute for Biological Studies, 10010 North Torrey Pines Road, La Jolla, CA 92037, USA

³The Sprott Centre for Stem Cell Research, Ottawa Hospital Research Institute, Ottawa, ON K1H 8L6, Canada

⁴The University of Toronto, Toronto, ON M5G 1L5, Canada

⁵Department of Molecular Hematology, University of Frankfurt Medical School, 60590 Frankfurt am Main, Germany

⁶Howard Hughes Medical Institute

⁷The Institute for Systems Biology, Seattle, WA, USA

⁸Institute of Molecular Pathology, 1030 Vienna, Austria

*Correspondence: josef.penninger@imba.oeaw.ac.at

DOI 10.1016/j.stem.2011.10.012

SUMMARY

All somatic mammalian cells carry two copies of chromosomes (diploidy), whereas organisms with a single copy of their genome, such as yeast, provide a basis for recessive genetics. Here we report the generation of haploid mouse ESC lines from parthenogenetic embryos. These cells carry 20 chromosomes, express stem cell markers, and develop into all germ layers *in vitro* and *in vivo*. We also developed a reversible mutagenesis protocol that allows saturated genetic recessive screens and results in homozygous alleles. This system allowed us to generate a knockout cell line for the microRNA processing enzyme Droscha. In a forward genetic screen, we identified Gpr107 as a molecule essential for killing by ricin, a toxin being used as a bioweapon. Our results open the possibility of combining the power of a haploid genome with pluripotency of embryonic stem cells to uncover fundamental biological processes in defined cell types at a genomic scale.

INTRODUCTION

Some organisms such as yeast or social insects are haploid, *i.e.*, they carry a single set of chromosomes (Otto and Jarne, 2001). Haploidy in yeast has been utilized to identify fundamental mechanisms of biology (Hartwell *et al.*, 1974). However, all somatic mammalian cells carry two copies of chromosomes (*i.e.* exhibit diploidy) that obscure mutational screens. Organisms with a single copy of their genome, such as yeast, provide a basis for genetic analyses where any recessive mutation of essential genes will show a clear phenotype due to the absence of a second gene copy (Hartwell *et al.*, 1974). It has been shown recently (Carette *et al.*, 2009, 2011a, 2011b) that haploid mammalian cells allow forward genetic screens. However, no somatic haploid cell has ever been reported in mammals, likely because

haploidy is incompatible with mammalian development (Latham *et al.*, 2002). To this date, haploidy has been achieved in fish embryonic stem cells (ESCs) (Yi *et al.*, 2009) and human KBM-7 leukemia cells (Carette *et al.*, 2009, 2011a; Kotecki *et al.*, 1999), and by electrofusion to generate hybrid cells (Yan *et al.*, 2000).

Here we show that it is possible to generate mammalian haploid ESC lines from parthenogenetic mouse blastocysts derived from activated oocytes. Such cells show stable growth over multiple passages, can be efficiently subcloned, differentiate at similar kinetics as diploid ESCs, and can maintain haploidy even upon initiation of differentiation. Moreover, we provide evidence that haploid ESCs can be readily utilized for reverse genetics and forward genetic screens. Our study provides the experimental framework for a system that carries the promise to combine functional genomics with mammalian stem cell biology.

RESULTS

Derivation of Haploid Cell Lines from Parthenogenetic Murine Blastocysts

Parthenogenetic embryos develop from haploid oocytes and thus contain only the maternal genome. However, all reported cell lines derived from parthenogenetic embryos carry a diploid set of chromosomes (Kaufman *et al.*, 1983). We hypothesized that haploid cells might still be present in parthenogenetic early embryos and that haploid ESCs could be derived from such blastocysts. To accomplish this, we activated oocytes from superovulated C57BL/6 × 129 F1 females by exposing them to 5% ethanol. Activated oocytes were then transferred into pseudopregnant recipients (Figure 1A). At embryonic day (ED) 3.5, compacted morulae and blastocysts were harvested and cultivated under conditions used to derive ESCs. FACS analysis showed that a small number of the parthenogenetically derived cells indeed displayed a reduced DNA content (Figure S1A available online). Several rounds of FACS purification of this population and subsequent expansion resulted in two independent cell lines derived from two distinct blastocysts, hereafter termed

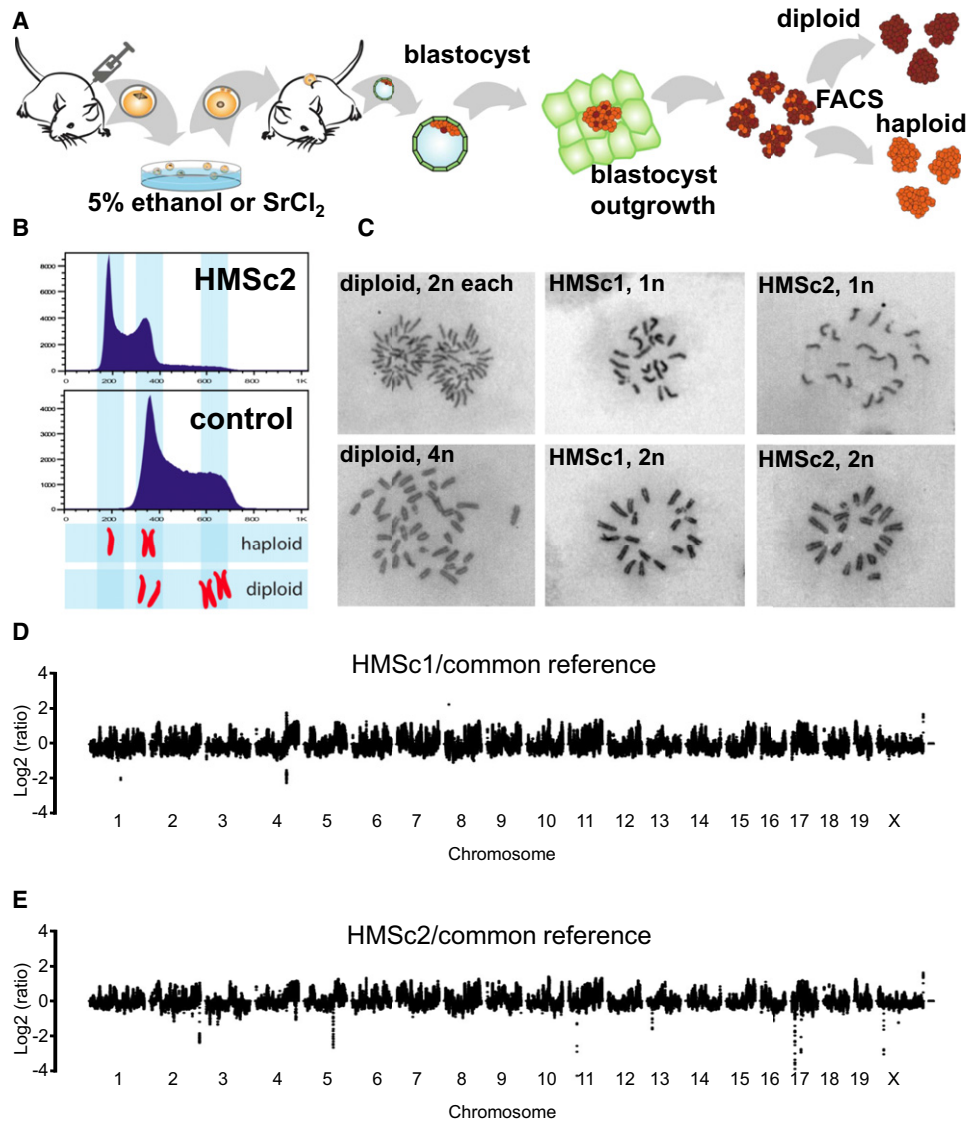


Figure 1. Generation of Haploid Murine ESC Lines

(A) Schematic overview of induction of parthenogenesis and the derivation of haploid ESC lines. Mouse oocytes were activated with either 5% ethanol [or 25 mM strontium chloride (SrCl₂)] and implanted into pseudopregnant females. ESCs were then generated from blastocysts and haploid cells subsequently sorted by FACS. Cultures were routinely resorted until we derived stable haploid cells.

(B) Flow cytometric analysis of DNA content in the control diploid ESC line IB10/C and the haploid HMSc2 cell line. DNA content was determined using Hoechst33342. 1n and 2n chromosome sets for haploid and 2n and 4n chromosome sets for diploid ESCs are indicated. The histograms show data from cells at the tenth sort.

(C) Representative chromosome spreads of control diploid ESCs and haploid HMSc1 and HMSc2 cells. Spreads from anaphase (1n) and prophase (2n) of mitosis are shown for haploid cells. As a control, anaphase (2n) and prophase (4n) spreads are shown for diploid ESCs.

(D and E) Sequence coverage relative to the common reference of parental in-house C57BL/6 and 129 strains is shown on a log₂ scale. Haploid cells were derived from C57BL/6 × 129 crosses. Chromosomes are arranged in numerical order and separated by small gaps.

See also Figure S1.

HMSc1 and HMSc2, with a 1n chromosome set in the G1 phase and a 2n chromosome set in the G2 phase of the cell cycle (Figure 1B, Figure S1A). Chromosome spreads showed that both cell lines carry a haploid set of 20 chromosomes (Figure 1C, Figure S1B). Of note, both cell lines have now been passaged >50 times without any signs of proliferative crisis. Thus, exploiting activation of meiotic oocytes and parthenogenetic derivation of

blastocysts has allowed us to establish mouse cells with a haploid chromosome set.

Genome Integrity

To genetically characterize our haploid cells, we compared their genomes to the genomes of the parental in-house mouse strains C57BL/6 and 129 using deep sequencing and performed

a discriminative coverage analysis. Briefly, we assessed the counts of sequencing reads, not counting duplicates that map to unique genomic positions, in a sliding window of 50 kb (10 kb offset), normalized to the total number of reads that mapped to the genome in each library. As expected, we found that the strains differed at many positions. We therefore compared deep sequencing reads from genomic DNA of both our haploid cell lines to both parental strains individually and in a combined fashion in which we focused on deviations with respect to both parental strain (Figures 1D and 1E). In total, we found that HMSc1 differed from the parental strains by more than 2-fold (multiple-testing corrected $p \leq 10^{-3}$) in 1,553 overlapping windows corresponding to 219 nonoverlapping regions; HMSc2 had 568 windows (113 regions) with increased read-counts and 61 windows (10 regions) with decreased read-counts (≥ 2 -fold; multiple-testing corrected $p \leq 10^{-3}$; Table S1 available online). Of note, 1,155 windows with increased read-counts and 99 windows with decreased read-counts overlapped between HMSc1 and HMSc2, while only 397 and 4 were distinct, respectively. We do not know the origin of this observation, but these shared copy number variations (CNVs) might stem from biases of the sequencing procedure during DNA preparation from different cell types (ESCs versus adult kidney), or they might constitute a batch effect during sequencing. Thus, taken together, our haploid cell lines display a limited number of defined CNVs compared with the parent strains, suggesting that they likely harbor small duplications and deletions, data similar to those of previous reports using established ESC (Baker et al., 2007) or iPSC (Hussein et al., 2011) lines.

To confirm that both haploid cell lines are indeed distinct given the similarity in copy number analysis, we made use of the fact that they were derived from oocytes of C57BL/6 \times 129 intercrosses, in that meiotic recombination should result in distinct haplotype structures. We compared the deep sequencing reads to small nucleotide polymorphisms (SNPs) obtained from the Sanger Institute release that differed between both mouse strains. Our sequences covered 1.5 million (HMSc2) and 1.7 million (HMSc1) distinct SNPs and allowed a unique assignment of the corresponding genomic regions to one of both parents. Comparing the SNPs present in HMSc1 and HMSc2 cells indeed confirmed that we had derived two independent haploid clones (Figure S1C). In summary, the CNV analysis together with FACS and chromosome spreads show that both cell lines are derived independently and exclude the possibility that HMSc1 and HMSc2 have substantial parts of the genome or individual chromosomes deleted or duplicated.

Expression of Prototypic ESC Markers

We next tested whether our haploid cell lines express prototypic ESC markers, i.e., whether our haploid cells are indeed ESCs. Both parthenogenetically derived haploid HMSc1 and HMSc2 lines exhibited typical morphologies of ESCs and stained positive for the ESC marker alkaline phosphatase (Figure 2A). Immunolabeling to detect Oct4, Nanog, and Sox2 (Figure 2B) confirmed that HMSc1 and HMSc2 cells express prototypic ESC markers. Transcriptome analysis showed that the expression profile for both haploid cell lines closely resembled that of the diploid ESC line IB10/C (Figure S2A). To focus on genes with the highest discriminatory value, we analyzed a set of 100 genes

for maximum difference in gene expression in either direction between mouse embryonic fibroblasts (MEFs) and diploid ESCs, among them *Nanog*, *Oct4*, and *Klf4* (Chambers et al., 2003). Analysis of this gene set showed that both HMSc1 and HMSc2 cell lines exhibit an expression signature that closely resembles that of the bona fide diploid ESC line IB10/C (Figure S2B, Table S2). qPCR analyses confirmed that both HMSc1 and HMSc2 cells express prototypic ESC markers (Figure 2C) (Elling et al., 2006; Takahashi and Yamanaka, 2006). Taken together, global transcriptome profiling and expression analysis of prototypic stem cell markers confirmed the ESC nature of both haploid cell lines.

Differentiation Potential of Haploid ESCs In Vitro

To test the differentiation potential of our haploid ESCs, we first assayed for embryoid body (EB) formation. Both haploid cell lines readily underwent EB formation and EB cells expressed the endodermal marker (Soudais et al., 1995) *Gata4* (Figure 2D). Differentiation was further confirmed using real time PCR. The prototypic ESC markers *Nanog*, *Rex1*, *Oct4*, *Sox2*, *Klf4*, *Sall4*, and *Klf2* (Chambers et al., 2003; Robertson et al., 1986; Takahashi and Yamanaka, 2006) were downregulated in EBs while mRNA expression of the lineage commitment markers (Zhang et al., 2010) *Hand1* (mesoderm and trophoderm), *Nkx2-5* and *Brachyury* (mesoderm), *Nestin* (neural), *Gata4*, *Gata6*, and *Foxa2* (all early endoderm), *Sox17* (endoderm and mesoderm), *Cxcr4R* (endoderm), and *Keratin18* (ectoderm) was upregulated relative to those of the parental haploid ESCs (Figure 2E, Figure S2C). These results indicate that the haploid ESCs are capable of differentiation into several lineages of all three germ layers.

In Vivo Differentiation Potential

To evaluate the ability of the established haploid ESC lines to contribute to adult mice, we injected cells from the Agouti⁺ ESC line HMSc2 into ED 3.5 blastocysts. To assure competitive growth and thus efficient contribution, diploid cells derived from haploid HMSc2 were used. Coat color chimerism was observed in 6 animals out of 25 mice born (Figure 3A). To analyze contribution of the entirely maternal-derived cells to various organs as previously reported for parthenogenotes (Thomson and Solter, 1988), we performed a distinguishing PCR and detected HMSc2-derived cells in multiple tissues (Figure S3A). To test the intrinsic differentiation potential of our haploid ESCs, we performed in vivo teratoma assays. Similar to diploid ESC controls, injection of both HMSc1 and HMSc2 cells always resulted in the formation of teratomas within 4–8 weeks.

In teratomas derived from both haploid ESC lines, we observed mesoderm-derived muscle cells, endoderm-derived Alcian-blue⁺ epithelial tissues that produce mucin, neuroectoderm-derived Tuj1⁺ neurons, and ectoderm-derived Cytokeratin 5⁺ epithelial tissues (Figure 3B). In addition, we observed bona fide cartilage tissue, fat, keratinized multilayered epithelium, pigmented epithelium, sebaceous sweat glands, glandular and neuronal tubules, and ciliated respiratory epithelium (Figures S3B–S3I). These data show that haploid ESC-derived cells have the potential to contribute to chimeric mice and that they can differentiate in vivo into cells of all three germ layers.

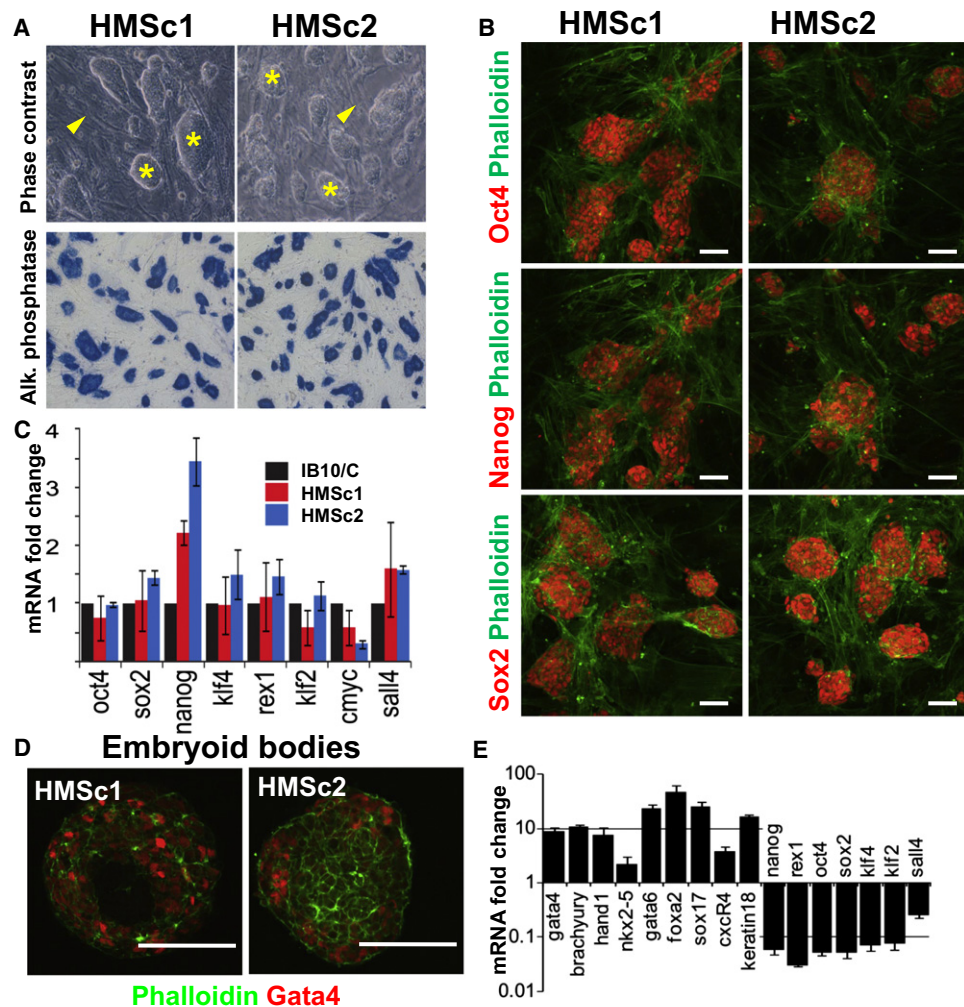


Figure 2. Marker Analysis and In Vitro Differentiation Potential of Haploid ESC Lines

(A) Both haploid HMSc1 and HMSc2 cell lines exhibit a morphology characteristic of ESC colonies (asterisk). Representative phase contrast images are shown. Note the feeder layer of mouse embryonic fibroblasts (MEF) (arrowheads). Haploid cells stain also positive for the ESC marker alkaline phosphatase (blue, bottom panels).

(B) Expression of Oct4, Nanog, and Sox2, prototypical markers for murine ESCs. Phalloidin staining indicates the feeder cell layer. Haploid HMSc1 and HMSc2 cells were costained for Oct4 (FITC) and Nanog (TRITC). In both cases, stainings are shown separately in the red channel. Scale bars are 50 μ m. Data are from cells after the fourth sort.

(C) Expression of prototypic ESC marker genes in the haploid HMSc1 (blue) and HMSc2 (red) cells. mRNA expression was determined using qPCR and normalized to diploid IB10/C ESCs (black bars). Mean and SD of three biological replicates (each done in triplicates) is shown.

(D) Gata4 protein expression in embryoid bodies (EB, day 7) as a marker for endoderm. Representative EBs are shown for both haploid HMSc1 and HMSc2 ESC lines counterstained with phalloidin (green). Scale bars are 50 μ m.

(E) qPCR revealed downregulation of the ESC markers Nanog, Rex1, Oct4, Sox2, Klf2, Klf4, and Sall4 in EBs (day 7) derived from the haploid ESC line HMSc2 accompanied by expression of the indicated lineage commitment markers (see text). mRNA expression was normalized to the parental, undifferentiated haploid ESCs (set at 1). Mean and SD of three biological replicates (each done in triplicates) is shown.

See also Figure S2.

The Ability of Stable Growth and Differentiation Is Intrinsic to Haploid ESCs

To assess whether our haploid ESCs have the intrinsic ability for stable growth, we established several individual cell clones by plating single haploid cells directly after FACS purification. These subclones were established in feeder-free conditions and were derived from both HMSc1 and HMSc2 parental lines that were previously cultured for more than 30 passages. All derived subclones expressed the stem cell markers Oct4 and Sox2 (Fig-

ure 4A, Figure S4) and formed EBs that contained Gata4⁺ endodermal cells and Tuj1⁺ neurons (Figure 4A, Figure S5). The haploid subclone HMSc2-27 was chosen for further studies based on its growth rates and numbers of stable haploid cells (Figures S6A and S6B).

Typical stem cell morphologies, protein expression of Oct4, Nanog, and Sox2, and a haploid set of chromosomes were confirmed for the HMSc2-27 subclone (Figures S6C–S6F). The growth rates of HMSc2-27 cells at different haploid:diploid

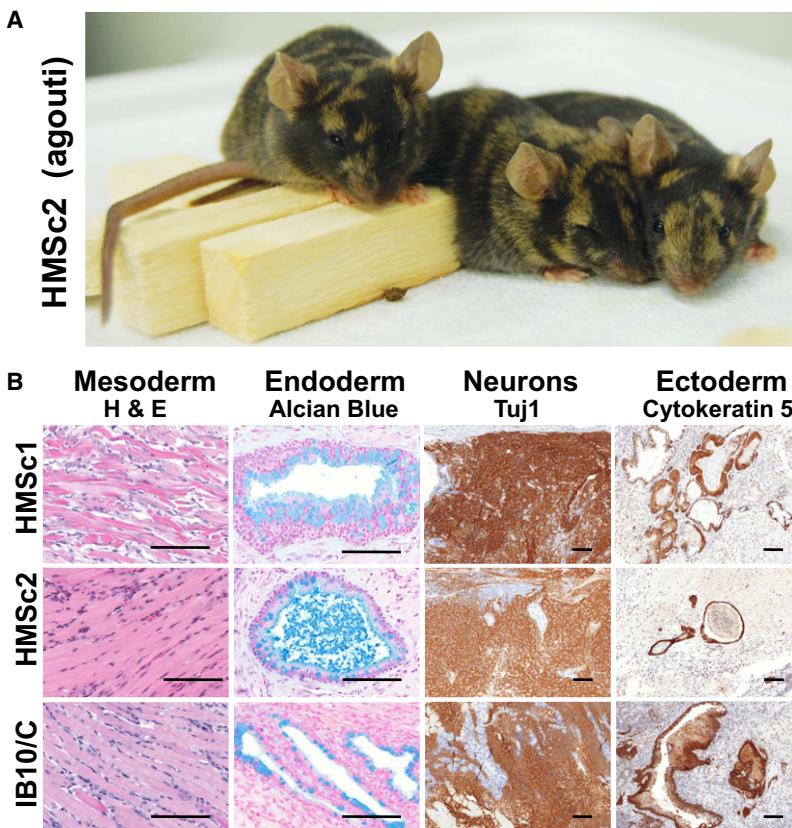


Figure 3. In Vivo Differentiation Potential of Haploid ESC Lines

(A) Haploid ESCs can contribute to tissues in adult mice. Diploid cells from the Agouti⁺ clone HMSc2 were injected into C57BL/6 blastocysts and coat color chimerism was observed (brown fur patches).

(B) Histological and immunohistochemical analysis of teratomas derived from control diploid IB10/C ESCs and the haploid ESC lines HMSc1 and HMSc2. Haploid ESCs can contribute to all three germ layers, namely muscle cells (H&E), intestinal endoderm (mucin-producing goblet cells stained by Alcian blue, counterstained with nuclear fast red), Tuj1⁺ neurons, and Cytokeratin 5 (K5)-expressing ectoderm. Tuj1⁺ and K5⁺ cells were detected by immunohistochemistry (DAB, brown), counterstained with hematoxylin (blue). Scale bars: 100 μ m. See also Figure S3.

differentiation we observed GFAP⁺ astrocytes and Tuj1⁺ neurons (Figure 5A and data not shown). We next tested whether differentiation and a state of haploidy are mutually exclusive, i.e., whether haploid cells need to become diploid before they differentiate. We therefore gated for the lineage markers Oct4 and Nestin in ESCs, NSCs, and differentiated NSC cultures and assayed cells for DNA content. Whereas nearly all Oct4⁺ cells remained haploid under all culture conditions, we observed haploid as well as diploid Nestin⁺ neural progenitor cells.

seeding ratios were comparable to those of purely diploid HMSc2-27 cells (Figure 4B). Of note, these growth rates are comparable to those of previously established ESC lines. Kinetic studies on diploid versus haploid cell ratios in cultures of HMSc2-27 cells showed that a large fraction of these cells maintains haploidy for a period of seven passages (Figure 4C). Differentiation of HMSc2-27 ESCs into EBs followed by lineage-specific differentiation protocols showed that these cells have the capability to form Gata4⁺ endoderm, Tuj1⁺ neuronal lineage (Figure 4A), and mesodermal “beating” myoblasts (Figure 4D; for synchronous contractions see Movie S1 and Movie S2). Moreover, in in vivo teratoma assays HMSc2-27 cells can differentiate into cells of all germ layers (not shown). To confirm the subcloning experiment, i.e., to make sure that cloning from a single haploid ESC indeed works, we generated GFP⁺ subclones. All cells from the established subclones expressed GFP, irrespective of whether they were at a stage of haploidy or diploidy (Figure 4E). Because diploid cells cannot become haploid, these experiments confirm that all cells of such clones must have been derived from a single haploid cell.

The HMSc2-27 subclone allowed us to examine the differentiation potential of these cells at a haploid versus diploid state. Haploid HMSc2-27 ESCs were indeed able to downregulate Oct4 and form Tuj1⁺ neurons and Gata4⁺ endodermal cells in EB cultures (Figure 4F). We next attempted to differentiate haploid HMSc27 cells directly (without formation of EBs) into neural and astrocyte lineages (Pollard et al., 2006). HMSc2-27 cells were able to differentiate into neural stem cells (NSCs) as defined by Nestin expression. Moreover, upon their further

However, when such neural progenitors were further differentiated toward astrocytes and neurons, all Nestin⁺ cells became diploid within 4 days (Figure 5B).

The differentiation capacity of haploid cells was further assessed using high content screening analysis of Oct4 expression (Walker et al., 2007, 2010), DAPI intensity, and nuclear area, enabling automated determination of the differentiation state of haploid and diploid HMSc2-27 cells (Figure S7). ESCs cultured in presence of LIF for 72 hr maintained high levels of Oct4 as depicted by mean Oct4 expression intensity (Figure 5C, left panel). Distribution analysis showed that HMSc2-27 cells that became diploid expressed a slightly higher level of Oct4 than haploid cells, consistent with the larger nucleus. Upon LIF withdrawal, Oct4 expression substantially decreased in haploid and diploid HMSc2-27 cells (Figure 5C, middle panel). Moreover, differentiation in response to 0.5 μ M retinoic acid dramatically reduced Oct4 expression in haploid and diploid HMSc2-27 cells to that of background levels (Figure 5C, right panel), similar to results obtained using 0.1 μ M retinoic acid (data not shown), indicating efficient differentiation. These data show that haploid ESCs can differentiate at kinetics similar to those of diploid ESCs and, importantly, that haploid stem cells can maintain haploidy even upon initiation of differentiation.

Retroviral Mutagenesis

The idea behind establishing haploid ESCs was to create a tool for forward and reverse genetics at the genomic scale. To demonstrate the power of mutagenesis in haploid mouse ESCs, we infected 5×10^8 cells of a freshly FACS-purified haploid culture

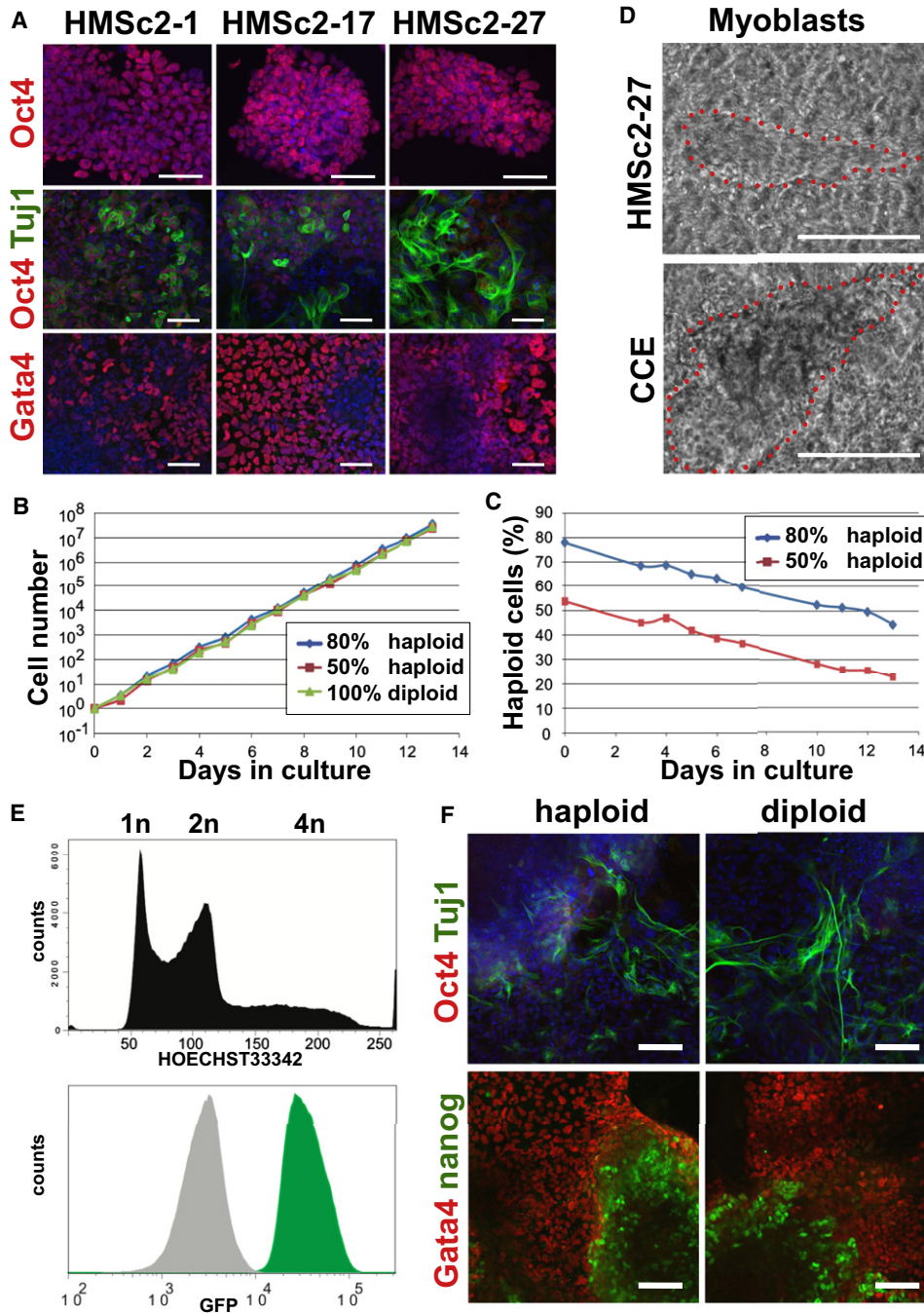


Figure 4. Haploid ESCs Have the Intrinsic Ability for Stable Growth and Differentiation

(A) Immunostaining for Oct4 protein expression (red) on three different subclones that were established by plating single haploid cells directly after FACS purification (top panels). The middle and bottom panels show immunostaining for Oct4 (red) and Tuj1 (green) expression and expression of the endodermal marker Gata4 (red, counterstained with DAPI) in attached EBs (day 10) derived from the indicated subclones. Data are from cells that were subcloned after >30 passages of the parental line. Scale bars are 50 μ m.

(B and C) Proliferation rates (B) and percentages of haploid cells (C) in control cultures containing 100% diploid HMSc2-27 cells and cultures of HMSc2-27 cells seeded at 80:20 and 50:50 ratios of haploid:diploid cells. Multiplication rates and percent haploidy were determined every 24 hr using FACS analysis of Hoechst33342-stained cells. Note that for this experiment cells were continuously kept in culture for 7 passages (14 days). Based on this experiment, we estimate that ~2%–3% of haploid cells became diploid each day over the course of the experiment. For both (B) and (C), mean and SD of three replicates is shown.

(D) Development of myoblasts from the haploid ESC subclone HMSc2-27. The feeder-cell-free diploid ESC line CCE was used as a control for this experiment. Representative phase contrast images are shown (see [Movie S1](#) and [Movie S2](#) to watch typical “beating” of these myoblasts). Scale bars are 100 μ m.

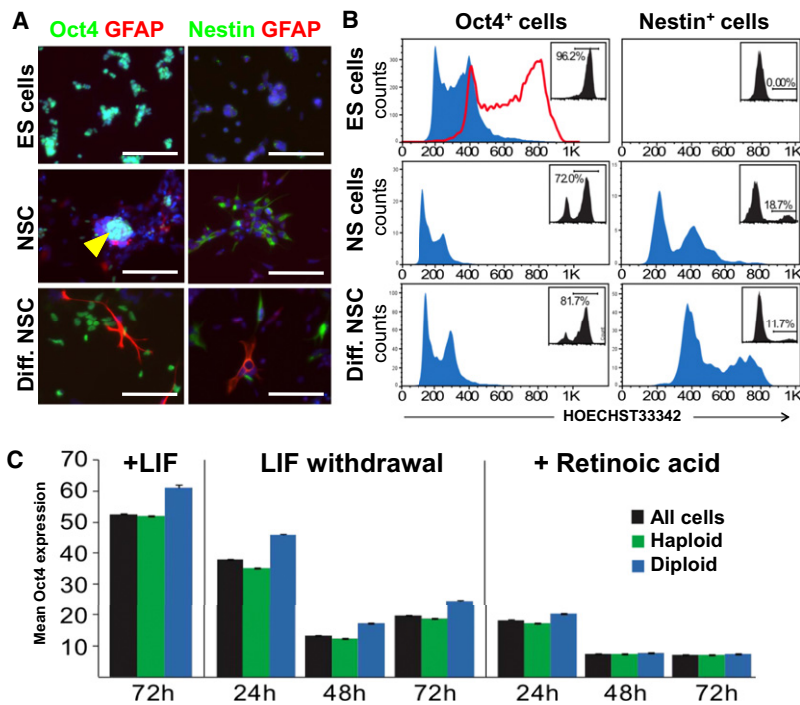


Figure 5. Differentiation Potential of Haploid ESCs

(A) Analysis of the haploid ESC clone HMSc2-27 cultured under conditions to maintain an ESC fate (ESCs), in vitro differentiated into Nestin⁺ neural stem cells (NSCs), and further differentiation into GFAP⁺ astrocytes by withdrawal of EGF and FGF2 in the presence of 1% serum (differentiated NSC culture conditions). Immunofluorescence labeling of Oct4, Nestin, and GFAP are shown, counterstained for DAPI. Representative images are shown. Scale bar is 100 μ m.

(B) Flow cytometry analysis of DNA content in cells gated for Oct4 and Nestin expression and grown under ESC (top), NS cell (middle), and differentiated NSC (bottom panels) conditions. The gates used and percentages of cells are inserted in each plot. Haploid cells are prominent in Oct4⁺ fractions under all conditions whereas Nestin⁺ cells differentiated for 4 days are devoid of haploid cells. The red line in the top left panel shows the representative DNA content of the diploid control IB10/C ESC line gated for Oct4 expression.

(C) Haploid cells exit the pluripotent state following the same dynamics as diploid cells. The left panel shows control Oct4 levels (mean intensity depicted) in haploid HMSc2-27, mixed (haploid and diploid) HMSc2-27, and control diploid CCE ESCs after 72 hr under control (plus LIF) conditions. Differentiation by LIF withdrawal leads to diminished Oct4 expression of diploid and haploid cells (middle panel). Differentiation induction using 0.5 μ M retinoic acid results in a rapid loss of Oct4 expression in both

haploid and diploid cells, indicative of differentiation (right panel). The same results were obtained when we used 0.1 μ M retinoic acid (not shown). Data are shown as mean Oct4 fluorescence intensity \pm SEM analyzing more than 50,000 cells per condition. One-way ANOVA ($p > 0.05$) showed increased expression of Oct4 in diploid cells (consistent with increased nuclear area) in all conditions except the 48 hr and 72 hr retinoic acid treatments wherein Oct4 expression was at background levels.

See also Figure S7.

of HMSc2-27 with a previously reported retrovirus containing a reversible gene trap (Schnütgen et al., 2008). This vector also contains removable Oct4 binding sites (Schnütgen et al., 2008), which allow insertions into genes that show minimal or no detectable expression in stem cells. After infection, 7.5×10^6 independent genomic insertions were generated as estimated from colony formation assays.

ESC colonies were then pooled and 10 μ g of genomic DNA corresponding to 3 million cells was analyzed to map the viral insertion sites by inverse PCR and deep sequencing. We could unambiguously identify 176,178 insertions. About half of the insertions were mapped to intergenic regions and \sim 51% of insertions occurred in promoter regions and intragenic regions encompassing 8,203 different genes (5' and 3' UTR, first intronic, other intronic, and coding regions) (Figure 6A). Among the intragenic insertions, approximately half (53%) were in the sense direction, and half were in the antisense direction. Of note, we observed frequent insertions into the first intron, which most likely will result in complete disruption of gene expression/function. To analyze gene trap efficacy, we divided genes into 10 bins based on their expression levels in HMSc2 cells (0%–10% equals lowest expression, and 90%–100% equals the most

highly expressed genes). As expected, more highly expressed genes were more often hit (up to 67%). Importantly, due to the engineered Oct4 binding sites (Schnütgen et al., 2008), we were able to obtain frequent (31%) insertions into genes that show minimal or no detectable expression in ESCs (Figure 6B). We next analyzed the numbers of genes that are trapped by all 176,178 insertions or fractions of the total insertions (Figure 6B; all insertions are set to 100% at the x axis). This analysis shows that mutagenesis has not reached saturation, indicating that higher numbers of insertions will increase the numbers of targeted genes. Considering that our library consists of $40 \times$ more (7.5×10^6) independent integrations, our mutagenesis protocol has, in principle, the power to disrupt most genes.

Haploid Murine ESCs as a Tool for High-Throughput Reverse Genetics

Using our retroviral mutagenesis set-up, we next picked individual clones, identified the insertion sites of about 1,000 cell lines (not shown), and selected 10 clones with sense or antisense insertions for further analysis. PCR analysis with site-specific primers confirmed that our sequencing approach identified the correct target sites in all 10 cases (Figure 6C). Most importantly

(E) GFP expression (green) in a GFP-tagged haploid ESC subclone. Non-GFP labeled cells are shown as control (gray shaded histogram). Flow cytometry of DNA content (Hoechst33342) is shown for the same subclone demonstrating that both haploid and diploid cells express GFP.

(F) Differentiation of haploid and diploid HMSc2-27 cells into EBs (day 13) that contain Tuj1 neurons (green) and Gata4-expressing endodermal cells (red). Note downregulation of Oct4 expression (red, upper panel) and the presence of residual clusters of Nanog⁺ cells (green, bottom panels). In the top panels, cells were counterstained with DAPI to visualize nuclei. Scale bar is 50 μ m. See also Figures S4–S6.

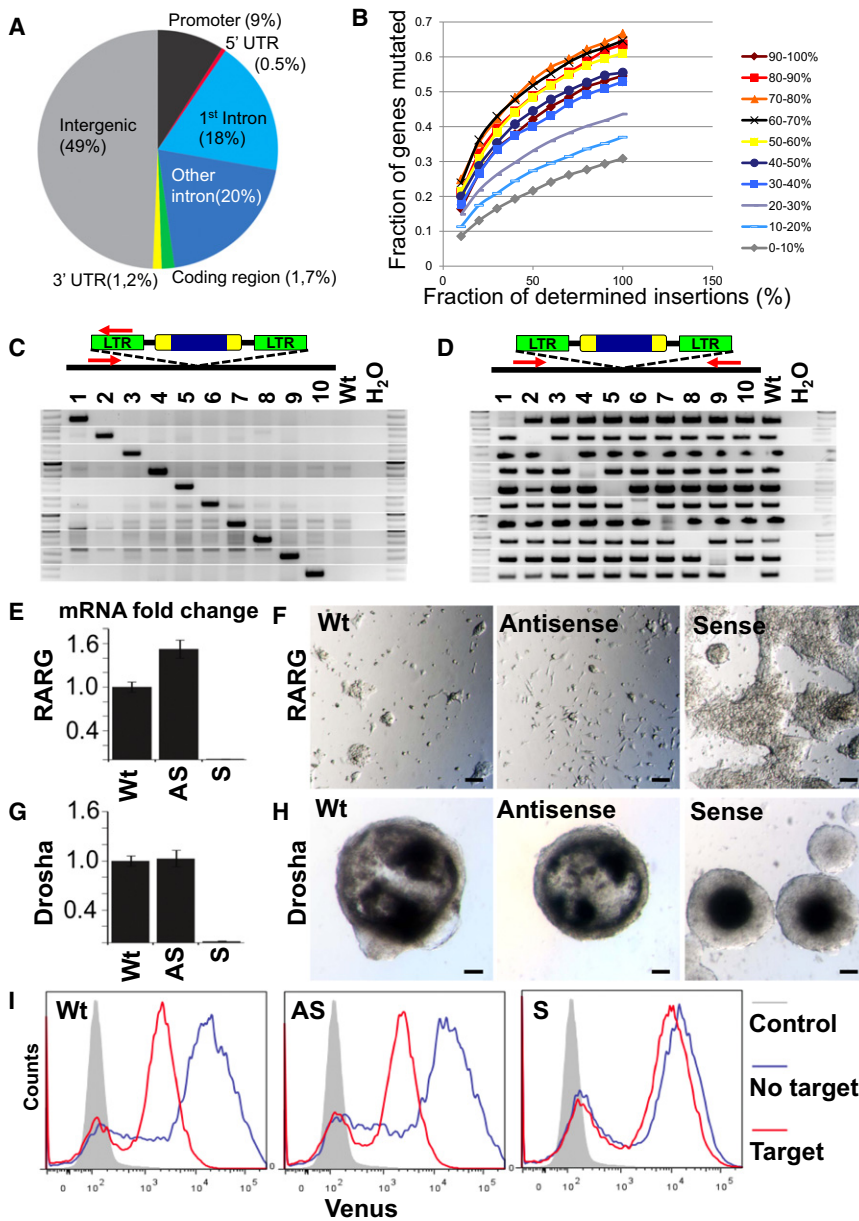


Figure 6. Reverse Genetics in Haploid ESCs

(A) Analysis of virus integration sites after neomycin selection. One-hundred seventy-six thousand, one-hundred seventy-eight insertions were determined by deep sequencing. The retrovirus landed in 49% intergenic and 51% intragenic regions, with a high frequency of integration into introns, especially the first intron.

(B) Graph shows percentage of genes with virus integrations following a single round of retroviral mutagenesis for different fractions of the total viral integration sites (x axis). Genes with the 10% lowest expression (0%–10%) showed the least integration efficiency, while more highly expressed genes (50%–100%) showed more efficient gene trapping. For increasing fractions of the total viral integration sites (x axis) higher saturation is reached, up to but not exceeding a saturation of 67%, indicating that additional genes are trapped in the total library of 7.5 million independent insertions.

(C and D) PCR analysis using site-specific primers for the indicated genes and a primer specific for the LTR of the inserted retrovirus. The location of the used PCR primers is schematically indicated on top of each panel. Of note, all primers were used for all 10 different genes showing (C) that the virus has indeed integrated into the site identified by initial sequencing and (D) that the integrations result in homozygous mutations of the respective loci. Lane 1 = *Madcam1*; lane 2 = *Drosha*; lane 3 = *Retinoic acid receptor gamma (Rarg)*; lane 4 = *Ap4s1*; lane 5 = *Arap1*; lane 6 = *Evx1*; lane 7 = *Bcl2l1*; lane 8 = *2210012G02RIK*; lane 9 = *Titin*; lane 10 = *Chr2:50928851*. Positive wild-type (WT) and negative H₂O controls are shown.

(E) qPCR analysis of RARG mRNA expression in haploid HMSC2-27 cells that are wild-type for *rarg* (WT), HMSC2-27 cells that contain the splice acceptor in antisense orientation (AS), and HMSC2-27 cells that contain the splice acceptor in the sense orientation (S). mRNA expression was normalized to the parental HMSC2-27 cells. Mean and SD of three replicates is shown.

(F) Representative images of cultures containing the indicated WT, antisense, and sense RARG HMSC2-27 cells treated with 0.1 μM retinoic acid for 10 days. Note the near complete absence of cells in the WT and antisense cultures. Scale bars are 100 μm.

(G) qPCR analysis of Drosha mRNA expression in haploid HMSC2-27 cells that are wild-type for *Drosha* (WT), HMSC2-27 cells that contain the splice acceptor in antisense orientation (AS), and HMSC2-27 cells that contain the splice acceptor in the sense orientation (S). mRNA expression was normalized to parental HMSC2-27 cells. Mean and SD of three replicates is shown.

(H) Complete absence of cystic EBs in *Drosha*-deficient HMSC2-27 cells as compared with Drosha-expressing WT HMSC2-27 cells and cells containing the splice acceptor in the antisense orientation. Representative images for EBs are shown on day 10 after EB induction. Of note, we did not observe a single cystic EB in *Drosha* mutant cells even in prolonged culture. Scale bars are 100 μm.

(I) Histograms showing Venus reporter gene expression in wild-type HMSC2-27 cells (WT), HMSC2-27 cells that contain the splice acceptor in antisense orientation (AS), and HMSC2-27 cells that contain the splice acceptor in the sense orientation (S) transduced with pSENSOR-based miRNA constructs harboring a potent shRNA targeting Firefly Luciferase with (target) or without (no target) its target site in the 3' UTR of Venus. Cells were gated on shRNA-expressing (dsRed⁺) cells and Venus expression levels were compared with nontransduced control cells (grey).

these data also show that all 10 clones carry homozygous insertions (Figure 6D), indicating that mutagenesis has occurred in haploid cells and that this approach is indeed feasible for recessive genetics.

Two clones carrying insertions in the genes encoding the retinoic acid receptor gamma (*Rarg*) and *Drosha* were function-

ally validated using parental wild-type (WT) HMSC2-27 cells, or ESCs clones that carry the retroviral vector in antisense orientation. By transient Cre expression we then converted the alleles to sense integrations in which the splice acceptor disrupts gene expression; this approach allows immediate confirmation of the candidate gene and excludes potential background

mutations. Indeed, sense, but not antisense, integrations of the splice acceptor results in a near complete absence of Rarg mRNA expression (Figure 6E). Functionally, whereas ESCs carrying the WT allele or the splice acceptors in antisense orientation undergo rapid differentiation and cell death upon retinoic acid treatment, disruption of Rarg expression renders ESCs insensitive to such retinoic acid effect (Figure 6F).

The RNase III Droscha catalyzes the conversion of pri-miRNA transcripts into pre-miRNA stem-loop precursors in the nucleus (Lee et al., 2003). Due to this pivotal role in the initial step of miRNA processing, homozygous Droscha inactivation is predicted to severely impair miRNA biogenesis. While a conditional Droscha knockout mouse has been published previously (Chong et al., 2008), no viable Droscha knockout cell line has been reported yet. We were indeed able to generate a Droscha mutant ESC clone following Cre-mediated inversion of the splice acceptor (Figure 6G). As reported for ESCs with mutations in the pasha ortholog Dgcr8 (Wang et al., 2007), which together with Droscha is part of a protein complex called the Microprocessor complex (Denli et al., 2004), Droscha mutant ESCs cannot form cystic EBs (Figure 6H). To evaluate primary miRNA processing in ESCs harboring the disrupted Droscha allele, we monitored the effects of a potent miR30-based shRNA (shmiR.Luc1309) on expression of a transcript harboring a Luc1309-specific shRNA target site (target) in the 3' UTR of a sequence encoding the Venus reporter protein (Fellmann et al., 2011). While expression of shmiR.Luc1309 strongly suppressed Venus expression in normal ESCs, our Droscha-deficient ESC clone did not show shRNA-mediated reporter suppression (Figure 6I), indicating a dysfunctional miRNA pathway. These data show that haploid ESCs can be indeed efficiently used for reverse genetics creating reversible and homozygous mutations.

A Genome-Wide Screen for Genes Involved in Ricin Toxicity

Finally, we set out to perform a recessive forward genetic screen at the genome level using our haploid ESC system. The naturally occurring ricin toxin from the castor oil plant *Ricinus communis* is highly poisonous. At the molecular level, ricin binds to N-acetyl galactosamine or beta-1,4-linked galactose residues and mannose receptors on the cell surface, and ricin molecules are thought to follow retrograde transport via the Golgi apparatus to enter the lumen of the endoplasmic reticulum (ER), where they escape into the cytosol to inactivate ribosomes (Spooner and Lord, 2011). Because we found that ricin is highly toxic to mouse ESCs, we used our mutagenized haploid HMSc2-27 cell library and challenged the cells with a lethal dose of ricin. Whereas ricin killed all control ESCs, we observed growth of multiple ESC colonies from the mutagenized haploid HMSc2-27 cells (Figure 7A). These clones were then pooled and deep sequenced so we could determine the integration sites. As expected from previous studies, we found multiple enzymes involved in sugar metabolism: *beta-1,4-galactosyltransferase 1* (*B4galt1*), *N-acetyllactosaminide beta-1,6-N-acetylglucosaminyltransferase* (*Gcmt2*), *polypeptide N-acetylgalactosaminyltransferase2* (*Galnt2*), *glycoprotein galactosyltransferase alpha 1,3* (*Ggta1*), and *polypeptide N-acetylgalactosaminyltransferase3* (*B4galnt3*) (Figures 7B and 7C). We also obtained multiple disruptive mutations in the alpha-(1,3)-fucosyltransferase *Fut9*, and we

hit the GDP-fucose transporter1 *Slc35c1* (Figure 7B and 7C). The fucosylation pathway has until now never been associated with ricin toxicity.

Intriguingly, we observed 49 different integrations in the GPCR *Gpr107* (*LUSTER1*) (Figure 7B), suggesting that *Gpr107* is a key molecule involved in ricin toxicity. Knockdown of *Gpr107* expression in HMSc2-27 cells using shRNA technology in HMSc2 confirmed the central role of this GPCR in ricin toxicity. The key role of *Gpr107* in ricin-induced cell death was further confirmed in a different cell type, NIH 3T3 cells (Figures 7D and 7E). Of note, our shRNA data are shown as ratios of viable cells recovered from the plates with ricin treatment to those without ricin treatment (% survival): around 1% of nontransduced or control shRNA-transduced cells remained still viable after 48 hr of ricin treatment, as compared with their respective nontreated cells; shRNA-mediated knockdown of *Gpr107* significantly enhanced survival of ricin-exposed HMSc2-27 and NIH 3T3 cells, but did not fully protect these cells from ricin toxicity. By contrast, genetic ablation of *Gpr107* in haploid HMSc2-27 ESCs as performed for the screen resulted in cells that survived ricin application for 3 weeks and were able to expand and form colonies starting from single, mutated cells. Thus, forward genetic screens are feasible and efficient in our haploid ESCs.

DISCUSSION

Our data show that it is possible to generate mammalian haploid ESC lines from parthenogenetic mouse blastocysts derived from ethanol-activated oocytes. In addition, we have now also successfully used strontium chloride to activate oocytes and derive a third independent haploid ESC line (not shown). Detailed molecular characterization of our haploid ESCs shows that these cells express all classical markers of diploid ESCs, carry 20 chromosomes, and largely maintain genome integrity. Functionally, these haploid ESCs can differentiate into cells from all three germ layers in vitro and in vivo. Although our lines and subclones are stable and in some cases have been maintained for over 70 passages, some haploid cells become diploid. Our mutagenesis data suggest that these cells do not become diploid via cell fusion, but rather via failed cytokinesis and/or endoreduplication of the genome. The exact mechanism needs to be determined. Moreover, it will be interesting to determine at what stage of development haploid cells have to become diploid to form a certain cell type, experiments that will be feasible using our high-throughput imaging platform that also allows us to track haploidy in a single cell.

Most importantly, our haploid ESCs can be mutated and, in all cases we have analyzed to date, these mutations are homozygous, indicating that such haploid cells can be used to analyze recessive and disease phenotypes in various cell lineages in vitro. Although we detected contributions of our cell lines to multiple tissues in vivo, it needs to be determined whether these haploid cells might be able to contribute to the germline. However, germline transmission could be attempted using semi-cloning techniques as previously reported for Medaka (Yi et al., 2009).

Our results open the possibility of combining the power of a haploid genome with pluripotency of ESCs. Recessive genetic screens have elucidated a wide variety of biological processes

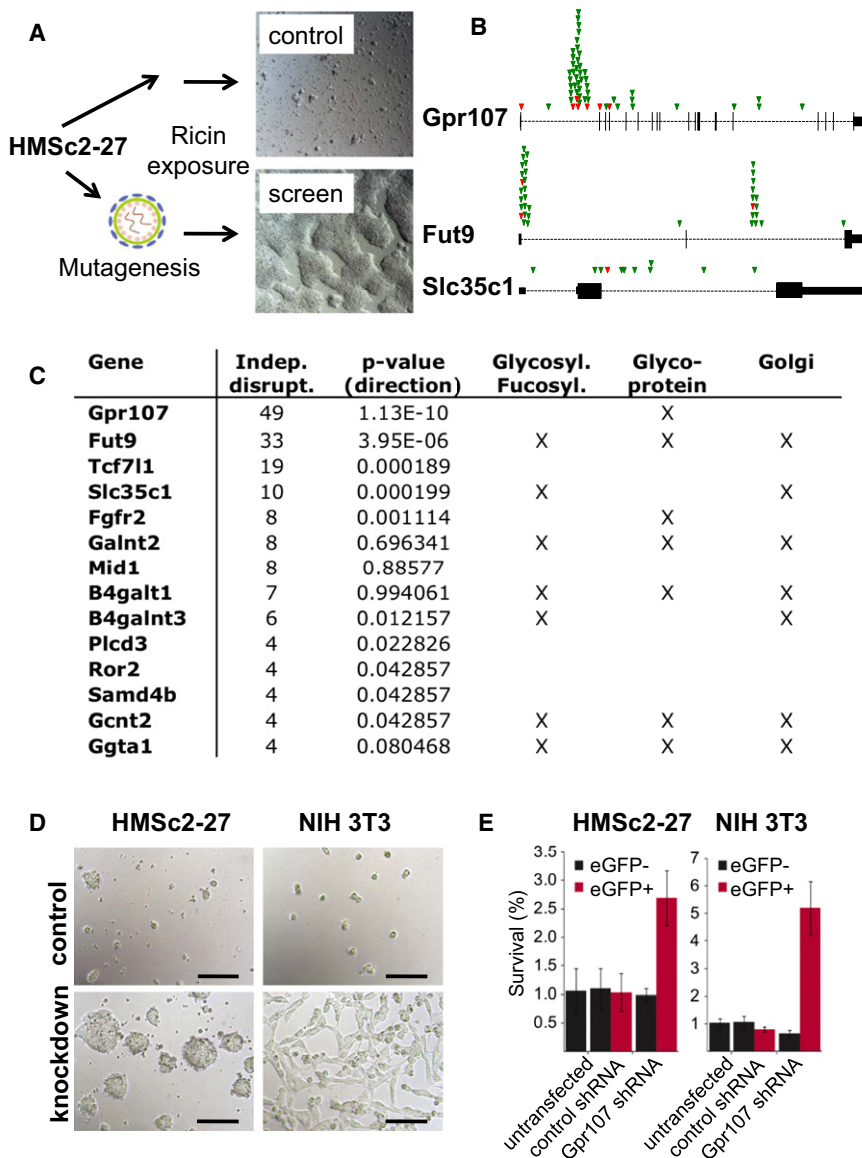


Figure 7. Forward Genetic Screen for Ricin Toxicity in Haploid ESCs

(A) Haploid HMSC2-27 cells with and without gene trap mutagenesis were exposed to ricin from *Ricinus communis* for 3 weeks. Colonies only appeared in the mutagenized batch and were processed for deep sequencing.

(B) Top hits identified in the ricin toxicity screen. Sense (green) and antisense (red) insertions in *Gpr107*, *Fut9*, and *Slc35c1* genomic loci are shown. The vertical lines indicate the respective exons for each gene with the first exon always moved to the left side of each diagram. Insertions in antisense might disrupt gene function, and sense integrations will do so in almost all cases. Note that nearly all insertions are in sense for the splice acceptor and that some antisense integrations map to exons, all of which should result in disruptive mutations. Considering that ~50% of intragenic insertions are sense and ~50% are antisense, these data also show that the screen has indeed strongly enriched for disruptive mutations ($p > 1.13e^{-10}$ for *Gpr107*; $p > 3.95e^{-6}$ for *Fut9*; $p > 0.000019$ for *Slc35c1*).

(C) Genes identified in the ricin toxicity screen. The numbers of distinct retroviral insertions predicted to disrupt gene expression (either because of intragenic regions containing the sense orientation of the splice acceptor, or because of sense and antisense integrations into exons) are indicated. Enrichment for sense mutations versus antisense integrations was assessed using a binomial test, and the respective p values are indicated. Of note, antisense integrations can also lead to gene disruption. Assigned biochemical pathways and allocation to the Golgi apparatus are also indicated.

(D and E) Validation of *Gpr107* in ricin toxicity. HMSC2-27 ESCs and NIH 3T3 cells were transfected with LMN constructs expressing *Gpr107* or control shRNAs together with GFP, and were then challenged with a lethal dose of ricin for 2 days. Images show representative cultures after 48 hr of ricin treatment (D). Scale bars are 100 μ m. (E) The ricin survival rate as a ratio between recovered cells of ricin-treated and ricin-untreated cells is shown in percentages (as determined by quanti-

tative FACS analysis of cells gated for viability by forward scatter, side scatter, and PI staining after 48 hr of ricin treatment). Cells were cultured in 10 cm dishes in triplicates and average survival \pm SD was determined for eGFP⁻ (not transfected) and eGFP⁺ haploid HMSC2-27 ESCs and NIH 3T3 cells for each plate. For (E), Mean and SD of three replicates is shown.

over the last century and thus markedly contributed to our understanding of normal development, basic physiology, and disease (Nüsslein-Volhard and Wieschaus, 1980). However, due to the asexual proliferation cycle, saturated genetic screens in mammals have not been possible in cell culture systems or feasible in vivo (Carette et al., 2009). RNAi-based approaches have therefore revolutionized functional genomics. However, in many cases RNAi-mediated gene silencing still suffers from variable knockdown, off-target effects, and transient silencing effects (Brummelkamp et al., 2002; Carpenter and Sabatini, 2004; Fellmann et al., 2011). Recently, genome-wide saturating genetic screens have been introduced to a human leukemia cell line with a near haploid chromosome set (Carette et al., 2009) and have been highly successful in, for example, eluci-

dating host factors of toxins or viruses (e.g., Carette et al., 2011b).

Our experiments based on millions of different integrations generated in a single round of retroviral infection of haploid ESCs show that it should be possible to perform saturated genetic recessive screens in mammalian ESCs and the many cell types that can be derived from them. We also report that reverse genetics is feasible using a vector system that provides immediate confirmation of gene function in the same clones using Cre-mediated conversion of the splice acceptor sites. Using this system we have indeed been able to functionally validate our approach using clones with conditional *Rarg* and *Droscha* mutations. Moreover, we performed a forward genetic screen for ricin toxicity, one of the most dangerous poisons

also being used/investigated as a biological weapon by governments. Ricin also gained notoriety for its potential use as toxin in bioterrorism (Papaloucas et al., 2008). This screen in haploid ESCs identified the GPCR Gpr107 as an essential molecule required for ricin-induced killing. Since no antitoxins are available for treatment of ricin poisoning, molecular inhibition of Gpr107 (and possibly other molecules identified by our screen) might be useful to alleviate ricin toxicity in vivo, a hypothesis that now needs to be tested. We anticipate that our haploid ESCs can bridge the power of haploid organisms such as yeast with rapid and whole-genome genetic forward screens in stem cells or any differentiated cell type that one can derive from our haploid mouse ESC lines.

EXPERIMENTAL PROCEDURES

Parthenogenetic Activation of Oocytes

Oocytes were collected and incubated in 5% ethanol for 5 min. Subsequently, viable oocytes were transferred into pseudopregnant mice and blastocysts were collected at ED 3.5.

Derivation of ESCs

Blastocysts were placed on a feeder-coated cell culture dish with ESC derivation medium as previously described (Bryja et al., 2006). Blastocyst outgrowths were trypsinized and replated on a feeder layer to allow ESC colony outgrowth.

Genomic Sequencing

Purified DNA from mouse kidney or ESCs was sheared by sonication and subjected to the Illumina adaptor ligation protocol and sequenced in Illumina HiSeq. Reads were mapped to the genome using bowtie.

Stem Cell Characterization

Cells were analyzed for the presence of stem cell markers using qPCR or immunofluorescent labeling and an enzymatic assay for alkaline phosphatase.

Differentiation

Cells were differentiated by withdrawal of LIF and EB formation or by direct neuronal differentiation (Pollard et al., 2006). For teratoma formation, cells were injected testicularly or subcutaneously into nude mice and teratoma growth was monitored. To generate chimeric mice, HMSc2 ESCs were injected into C57BL/6 ED 3.5 blastocysts, and transferred into pseudopregnant females. Percentage chimerism was determined by coat color.

Retroviral Infection of ESCs and Inverse PCR

Virus was packaged in Platinum E cells. Selection for gene trap insertions was done using G418. The protocol for inverse PCR was adapted based on Carette et al. (2011a).

Ricin Toxicity Screen

A mutated library of cells was exposed to a lethal dose of ricin for 3 weeks. DNA of surviving cells was purified, subjected to inverse PCR, and analyzed by deep sequencing. For confirmation using shRNA knockdowns, cells were exposed to ricin for 48 hr and survival was quantified using FACS.

ACCESSION NUMBERS

The microarray data have been deposited in ArrayExpress with accession number E-MEXP-3294. All the primary sequencing data are available from GEO with the accession number SRA047251 for CNV analysis and GSE33184 for retroviral integration site analysis. Furthermore, primary and processed data is accessible at http://www.starklab.org/data/elling_CSC_2011/ and formatted for uploading to the UCSC genome browser (<http://genome.ucsc.edu/>).

SUPPLEMENTAL INFORMATION

Supplemental Information for this article includes Supplemental Experimental Procedures, Figures S1–S7, Tables S1 and S2, and Movies S1 and S2 and can be found with this article online at doi:10.1016/j.stem.2011.10.012.

ACKNOWLEDGMENTS

We would like to thank all members of our laboratories, in particular Dr. Wing Chang, for helpful discussions. Funding was provided by the Canadian Institutes for Health Research (MOP-89910) to W.L.S. W.L.S. is funded by a Canada Research Chair in Integrative Stem Cell Biology. U.E. was supported by a grant from the FWF (Project I434-B13). G.W. and D.S. were funded from the European Community's Seventh Framework Programme (FP7/2007-2013) under grant agreement n° 223151 - INFLA-CARE. A.S. is supported by a European Research Council (ERC) Starting Grant from the European Community's Seventh Framework Programme (FP7/2007-2013)/ERC grant agreement no. 242922. J.M.P. is supported by grants from IMBA, the Austrian Ministry of Sciences, and the Austrian Academy of Sciences, GEN-AU (Austro-Mouse), and by an EU ERC Advanced Grant. This work was supported, in part, by the Howard Hughes Medical Institute and a grant from the Gordon and Betty Moore foundation to J.R.E. J.R.E. is an HHMI-GBMP Investigator. We thank B. Zuber for helpful discussions and pathologic examination of teratomas. We are grateful to Thijn Brummelkamp for valuable discussions to establish retrovirus-based genome-wide mutagenesis. We thank all IMBA service units, especially Biooptics, the VBC Genomics unit, and the Transgenic Service, for technical support with this project. The ricin hits are currently being evaluated for patent protection.

Received: October 5, 2011

Revised: October 19, 2011

Accepted: October 21, 2011

Published: December 1, 2011

REFERENCES

- Baker, D.E., Harrison, N.J., Maltby, E., Smith, K., Moore, H.D., Shaw, P.J., Heath, P.R., Holden, H., and Andrews, P.W. (2007). Adaptation to culture of human embryonic stem cells and oncogenesis in vivo. *Nat. Biotechnol.* 25, 207–215.
- Brummelkamp, T.R., Bernards, R., and Agami, R. (2002). A system for stable expression of short interfering RNAs in mammalian cells. *Science* 296, 550–553.
- Bryja, V., Bonilla, S., and Arenas, E. (2006). Derivation of mouse embryonic stem cells. *Nat. Protoc.* 1, 2082–2087.
- Carette, J.E., Guimaraes, C.P., Varadarajan, M., Park, A.S., Wuethrich, I., Godarova, A., Kotecki, M., Cochran, B.H., Spooner, E., Ploegh, H.L., and Brummelkamp, T.R. (2009). Haploid genetic screens in human cells identify host factors used by pathogens. *Science* 326, 1231–1235.
- Carette, J.E., Guimaraes, C.P., Wuethrich, I., Blomen, V.A., Varadarajan, M., Sun, C., Bell, G., Yuan, B., Muellner, M.K., Nijman, S.M., et al. (2011a). Global gene disruption in human cells to assign genes to phenotypes by deep sequencing. *Nat. Biotechnol.* 29, 542–546.
- Carette, J.E., Raaben, M., Wong, A.C., Herbert, A.S., Obernosterer, G., Mulherkar, N., Kuehne, A.I., Kranzusch, P.J., Griffin, A.M., Ruthel, G., et al. (2011b). Ebola virus entry requires the cholesterol transporter Niemann-Pick C1. *Nature* 477, 340–343.
- Carpenter, A.E., and Sabatini, D.M. (2004). Systematic genome-wide screens of gene function. *Nat. Rev. Genet.* 5, 11–22.
- Chambers, I., Colby, D., Robertson, M., Nichols, J., Lee, S., Tweedie, S., and Smith, A. (2003). Functional expression cloning of Nanog, a pluripotency sustaining factor in embryonic stem cells. *Cell* 113, 643–655.
- Chong, M.M., Rasmussen, J.P., Rudensky, A.Y., and Littman, D.R. (2008). The RNaseIII enzyme Drosha is critical in T cells for preventing lethal inflammatory disease. *J. Exp. Med.* 205, 2005–2017.

- Denli, A.M., Tops, B.B., Plasterk, R.H., Ketting, R.F., and Hannon, G.J. (2004). Processing of primary microRNAs by the Microprocessor complex. *Nature* 432, 231–235.
- Elling, U., Klasen, C., Eisenberger, T., Anlag, K., and Treier, M. (2006). Murine inner cell mass-derived lineages depend on *Sall4* function. *Proc. Natl. Acad. Sci. USA* 103, 16319–16324.
- Fellmann, C., Zuber, J., McJunkin, K., Chang, K., Malone, C.D., Dickens, R.A., Xu, Q., Hengartner, M.O., Elledge, S.J., Hannon, G.J., and Lowe, S.W. (2011). Functional identification of optimized RNAi triggers using a massively parallel sensor assay. *Mol. Cell* 41, 733–746.
- Hartwell, L.H., Culotti, J., Pringle, J.R., and Reid, B.J. (1974). Genetic control of the cell division cycle in yeast. *Science* 183, 46–51.
- Hussein, S.M., Batada, N.N., Vuoristo, S., Ching, R.W., Autio, R., Närvä, E., Ng, S., Sourour, M., Hämmäläinen, R., Olsson, C., et al. (2011). Copy number variation and selection during reprogramming to pluripotency. *Nature* 471, 58–62.
- Kaufman, M.H., Robertson, E.J., Handyside, A.H., and Evans, M.J. (1983). Establishment of pluripotential cell lines from haploid mouse embryos. *J. Embryol. Exp. Morphol.* 73, 249–261.
- Kotecki, M., Reddy, P.S., and Cochran, B.H. (1999). Isolation and characterization of a near-haploid human cell line. *Exp. Cell Res.* 252, 273–280.
- Latham, K.E., Akutsu, H., Patel, B., and Yanagimachi, R. (2002). Comparison of gene expression during preimplantation development between diploid and haploid mouse embryos. *Biol. Reprod.* 67, 386–392.
- Lee, Y., Ahn, C., Han, J., Choi, H., Kim, J., Yim, J., Lee, J., Provost, P., Rådmark, O., Kim, S., and Kim, V.N. (2003). The nuclear RNase III Drosha initiates microRNA processing. *Nature* 425, 415–419.
- Nüsslein-Volhard, C., and Wieschaus, E. (1980). Mutations affecting segment number and polarity in *Drosophila*. *Nature* 287, 795–801.
- Otto, S.P., and Jarne, P. (2001). Evolution. Haploids—hapless or happening? *Science* 292, 2441–2443.
- Papaloucas, M., Papaloucas, C., and Stergioulas, A. (2008). Ricin and the assassination of Georgi Markov. *Pak. J. Biol. Sci.* 11, 2370–2371.
- Pollard, S.M., Benchoua, A., and Lowell, S. (2006). Neural stem cells, neurons, and glia. *Methods Enzymol.* 418, 151–169.
- Robertson, E., Bradley, A., Kuehn, M., and Evans, M. (1986). Germ-line transmission of genes introduced into cultured pluripotential cells by retroviral vector. *Nature* 323, 445–448.
- Schnütgen, F., Hansen, J., De-Zolt, S., Horn, C., Lutz, M., Floss, T., Wurst, W., Noppinger, P.R., and von Melchner, H. (2008). Enhanced gene trapping in mouse embryonic stem cells. *Nucleic Acids Res.* 36, e133.
- Soudais, C., Bielinska, M., Heikinheimo, M., MacArthur, C.A., Narita, N., Saffitz, J.E., Simon, M.C., Leiden, J.M., and Wilson, D.B. (1995). Targeted mutagenesis of the transcription factor *GATA-4* gene in mouse embryonic stem cells disrupts visceral endoderm differentiation in vitro. *Development* 121, 3877–3888.
- Spooner, R.A., and Lord, J.M. (2011). How Ricin and Shiga Toxin Reach the Cytosol of Target Cells: Retrotranslocation from the Endoplasmic Reticulum. *Curr. Top. Microbiol. Immunol.*, in press. Published online July 15, 2011. 10.1007/82_2011_154.
- Takahashi, K., and Yamanaka, S. (2006). Induction of pluripotent stem cells from mouse embryonic and adult fibroblast cultures by defined factors. *Cell* 126, 663–676.
- Thomson, J.A., and Solter, D. (1988). The developmental fate of androgenetic, parthenogenetic, and gynogenetic cells in chimeric gastrulating mouse embryos. *Genes Dev.* 2, 1344–1351.
- Walker, E., Ohishi, M., Davey, R.E., Zhang, W., Cassar, P.A., Tanaka, T.S., Der, S.D., Morris, Q., Hughes, T.R., Zandstra, P.W., and Stanford, W.L. (2007). Prediction and testing of novel transcriptional networks regulating embryonic stem cell self-renewal and commitment. *Cell Stem Cell* 1, 71–86.
- Walker, E., Chang, W.Y., Hunkapiller, J., Cagney, G., Garcha, K., Torchia, J., Krogan, N.J., Reiter, J.F., and Stanford, W.L. (2010). Polycomb-like 2 associates with PRC2 and regulates transcriptional networks during mouse embryonic stem cell self-renewal and differentiation. *Cell Stem Cell* 6, 153–166.
- Wang, Y., Medvid, R., Melton, C., Jaenisch, R., and Blöchl, R. (2007). DGCR8 is essential for microRNA biogenesis and silencing of embryonic stem cell self-renewal. *Nat. Genet.* 39, 380–385.
- Yan, H., Papadopoulos, N., Marra, G., Perrera, C., Jiricny, J., Boland, C.R., Lynch, H.T., Chadwick, R.B., de la Chapelle, A., Berg, K., et al. (2000). Conversion of diploidy to haploidy. *Nature* 403, 723–724.
- Yi, M., Hong, N., and Hong, Y. (2009). Generation of medaka fish haploid embryonic stem cells. *Science* 326, 430–433.
- Zhang, K., Li, L., Huang, C., Shen, C., Tan, F., Xia, C., Liu, P., Rossant, J., and Jing, N. (2010). Distinct functions of BMP4 during different stages of mouse ES cell neural commitment. *Development* 137, 2095–2105.